

# Floating Offshore Wind Turbine Dynamics: Large-Angle Motions in Euler-Space

**Bert Sweetman**  
Texas A&M University

**Lei Wang**  
Texas A&M University

**Abstract:** Floating structures have been proposed to support offshore wind turbines in deep water, where environmental forcing could subject the rotor to meaningful angular displacements in both precession and nutation, offering design challenges beyond conventional bottom-founded structures. This paper offers theoretical developments underlying an efficient methodology to compute large-angle rigid body rotations of a floating wind turbine in the time domain. The tower and rotor-nacelle assembly (RNA) are considered as two rotational bodies in the space, for which two sets of Euler angles are defined and used to develop two systems of Euler dynamic equations of motion. Transformations between the various coordinate systems are derived to enable solution for motion of the tower with gyroscopic, environmental and restoring effects applied as external moments. An example is presented in which the methodology is implemented in MATLAB to simulate time-histories of a floating tower with RNA.

## Nomenclature

- $(X, Y, Z)$  Translating non-rotating coordinate system with respect to the earth, with the origin  $O$  fixed at the center of mass of the tower
- $(x, y, z)$  Translating rotating coordinate system with the origin  $O$  fixed at the center of mass of the tower; the  $z$ -axis is fixed on the centerline of the tower while the  $x$ - and  $y$ -axes rotate about the  $z$ -axis independent of body rotations about that axis.
- $(X_n, Y_n, Z_n)$  Translating non-rotating coordinate system with respect to the earth, with the origin  $O'$  fixed at the center of mass of the RNA
- $(A, B, C)$  Translating rotating coordinate system with the origin  $O'$  fixed at the center of mass of the RNA
- $B$ -axis Spinning axis of the blades
- $B_p$ -axis Horizontal projection of the  $B$ -axis on the  $XOY$  plane
- $y_p$ -axis Horizontal projection of the  $y$ -axis on the  $XOY$  plane
- $(\theta_1, \theta_2, \eta)$  Three 3-1-3 sequence Euler angles used to describe the rotation of the tower, where  $\theta_1$  is measured from the  $Z$ -axis to the  $z$ -axis with the positive direction right-handed along the  $x$ -axis;  $\theta_2$  is measured from the  $X$ -axis to the  $x$ -axis with positive right-handed along the  $Z$ -axis;  $\eta$  is rotation along the  $z$ -axis with positive right-handed along the  $z$ -axis.
- $(\phi, \theta, \psi)$  Three 3-1-3 sequence Euler angles used to describe the rotation of the RNA, also called precession, nutation and spin angles, where  $\phi$  is measured from the  $Y$ -axis to the  $B_p$ -axis with the positive direction along the  $Z$ -axis;  $\theta$  is measured from the  $Z$ -axis to the  $B$ -axis with the positive direction along the  $C$ -axis;  $\psi$  is the spinning around the  $B$ -axis with the positive direction along the  $B$ -axis.
- $\lambda$  Measured from the  $B_p$ -axis to the  $B$ -axis with positive right-handed along the  $C$ -axis
- $\alpha$  Measured from the  $y_p$ -axis to the  $B_p$ -axis with positive right-handed along the  $Z$ -axis
- $\vec{\Omega}$  The angular velocity of the  $(A, B, C)$  coordinate system relative to  $(X, Y, Z)$
- $\vec{\omega}$  The angular velocity of the RNA relative to  $(X, Y, Z)$
- $C_T$  Thrust coefficient, used to calculate wind force on the blade swept area

## 1 Introduction and Background

Environmental, aesthetic and political pressures continue to push for siting offshore wind turbines beyond sight of land, where waters tend to be deeper, and use of floating structures is likely to be considered. Highly compliant floating support structures allowing large angular displacements are likely to be very cost-competitive for deep water. The increased

compliance of these structures will make simulation of system dynamics more challenging and important mainly because of effects of gyroscopic moments. For conventional, stiff, bottom-founded structures, these moments are primarily generated by mechanical precession of the spin axis into the shifting winds, and so are limited by the maximum yaw rate [1]. However, no such limit exists for gyroscopic moments of floating structures because they result from irregular motions of the tower.

A practical need for large-angle wind-turbine dynamics did not exist before the advent of floating offshore turbine structures. Conventional methods applicable to small-angle motions have been widely applied to dynamic analysis of offshore structures [2], including offshore wind turbines [3]. A fully coupled version of the NREL FAST aero-elastic simulator [4] is available to compute the dynamics of floating wind turbines using hydrodynamic forces computed using WAMIT [5]. FAST solves the equations of motion using transformation matrices made orthogonal by the Frobenius norm, which provides good results for angles not exceeding about 20 degrees [6]. In the work presented here, derivation of the rotational equations of motion in terms of Euler angles eliminates the need for small-angle approximations and mathematical normalization of transformation matrices.

Here, the system dynamics of a wind turbine structure are solved as a two-body problem; numerous other solution techniques for multi-body problems are available. To mention a few, Stoneking [7] presents the derivation of the exact nonlinear dynamic equations of motion for a multi-body spacecraft connected by spherical gimbal joints. Saha [8] derives the constrained dynamic equations of motion using the decoupled natural orthogonal complement matrices for a serial kinematic chain composed of rigid bodies. H. Matsukuma et al. (2008) [9] employ multi-body dynamic system theory to analyze the dynamic response of a 2 MW downwind turbine mounted on a spar-type floating platform for pitch amplitudes up to around 10 degrees in steady wind, but no waves, and conclude that the platform motions are considerably influenced by gyro moments associated with rotor rotation. In the method developed here, a reduction in the number of equations of motion enables enhanced numerical efficiency.

The tower and RNA are each considered as rotational bodies in the space, each described by a set of Euler's equations of motion. The RNA represents a combination of spinning and non-spinning parts, the latter being treated as a point-mass on the spin axis. The number of degrees of freedom is reduced by using geometry of the physical connection between these bodies. These new developments enable simulation of the two-body tower-RNA system using only one set of dynamic equations in Euler space. The effectiveness of the new theory is shown in an example in which the new methodologies are implemented in a MATLAB program to solve the equations of motion of a floating wind turbine subject to both irregular environmental forcing and gyro moments.

## 2 Coordinate Systems and Euler angles

The methodology considers the system as two rigid bodies: the tower is the complete structural assembly, including the buoyant hull, that supports the RNA; the RNA is the complete assembly that can mechanically yaw relative to the tower. Coordinate systems  $(X, Y, Z)$  and  $(x, y, z)$  both originate at the center of mass of the moving tower (Fig. 1). The  $(X, Y, Z)$  system is non-rotating, while  $(x, y, z)$  is a rotating coordinate system. The  $z$ -axis defines the center of the moving tower; the directions of  $x$  and  $y$  are not fixed to the tower. Angular differences between these coordinate systems define a set of independent Euler angles,  $(\theta_1, \theta_2, \eta)$ . The angle  $\theta_1$  lies between the vertical  $Z$ , and the tower centerline,  $z$ , with positive rotations right-handed about the positive  $x$ -axis. Angle  $\theta_2$  lies between  $Y$  and  $y_p$  with positive right-handed along positive  $Z$ -axis, and corresponds to the tower revolving around  $Z$ ;  $y_p$  is the projection of  $y$  on the horizontal  $X$ - $Y$  plane, and opposite to the projection of  $z$  onto  $X$ - $Y$ . The first two Euler angles,  $\theta_1$  and  $\theta_2$ , fully define the location of the  $(x, y, z)$  coordinate system. A third Euler angle,  $\eta$ , describes rotation about the moving  $z$ -axis, with positive rotations being right-handed about positive  $z$ .

For large angular displacements in space, the order in which the angles of rotation are applied is important; there are twelve possible Euler angles sequences. Here, 3-1-3 sequenced angles are used to describe the position of the rotating tower and of the spinning RNA (e.g., [10]). For the tower, a 3-1-3 sequence indicates the Euler sequence is  $z$ - $x$ - $z$ , or in detail: 1) first, rotate the upright tower about the  $z$ -axis (then coincident with  $Z$ ) through an angle  $\theta_2$  measured in the horizontal plane  $XOY$ ; 2) next, rotate the resultant tower about the resulting  $x$ -axis through an angle  $\theta_1$  measured in the vertical plane  $ZOy_p$ , and 3) finally, rotate the tower about the new  $z$ -axis (not coincident with  $Z$  for non-zero  $\theta_1$ ) through the third Euler angle,  $\eta$ . The Euler equations of motion of the combined tower and RNA (single-body case) or the tower alone (two-body case) are derived and solved in terms of  $\theta_2$ ,  $\theta_1$ , and  $\eta$ . This combination enables considerable simplification in the derivation of Euler's kinematic equations, which in turn results in dramatically simpler equations of motion, and improved numerical efficiency.

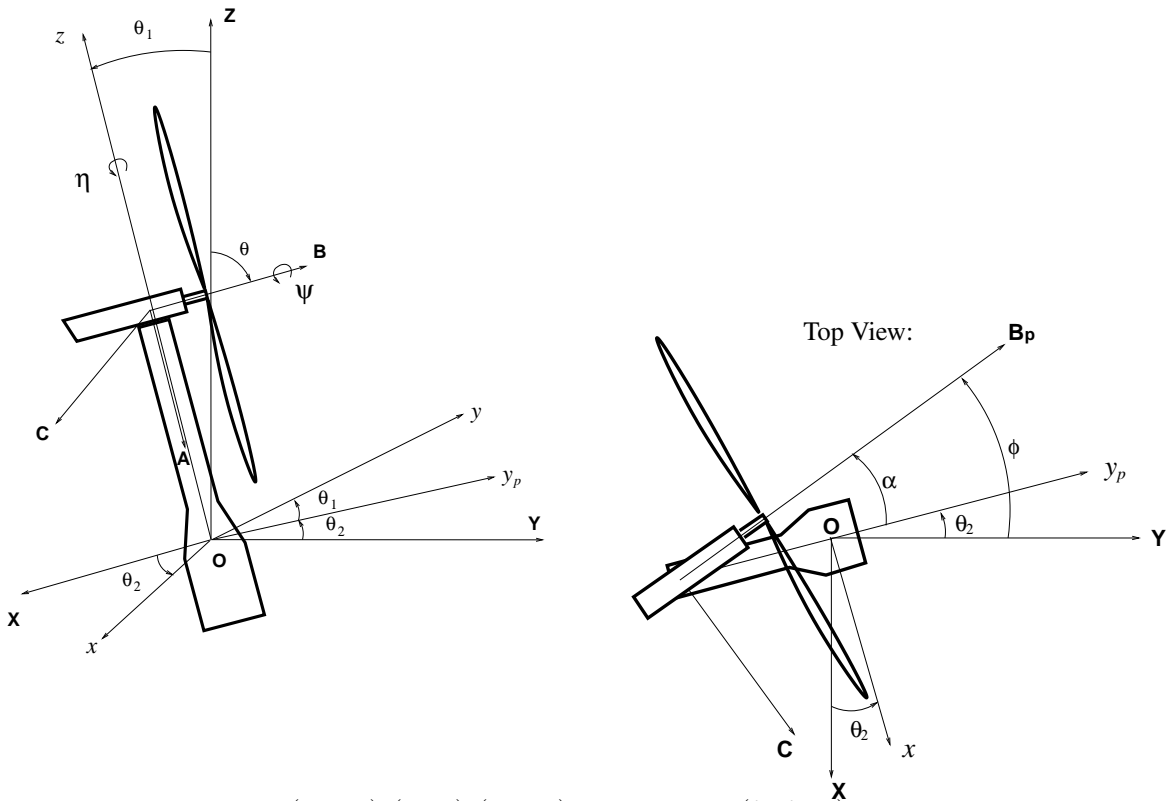


Fig. 1. Coordinate Systems:  $(X, Y, Z)$ ,  $(x, y, z)$ ,  $(A, B, C)$  and Euler angles  $(\theta_1, \theta_2, \eta)$ . Axis  $A$  shown slightly offset from  $z$  for clarity.

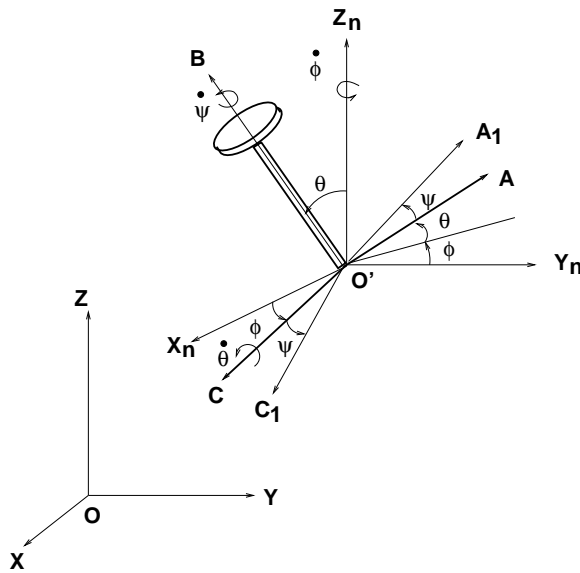


Fig. 2. Rotation of  $(A, B, C)$  in terms of  $\phi$ ,  $\theta$  and  $\psi$

Additional axes and angles are necessary to describe the position of the RNA. The translating coordinate system  $(X_n, Y_n, Z_n)$  and the rotating system  $(A, B, C)$  are used to form a second set of Euler angles, which is associated with the rotating machinery at the top of the tower. The origin of the disk-based  $(A, B, C)$  coordinate system is fixed at the center of mass of the RNA, here assumed to be at the intersection of the spin axis ( $B$ ) and the yaw axis ( $z$ ). The  $A$ -axis is generally not exactly parallel to  $z$  (Eqn. (5)). The angle  $\alpha$  is the difference between the  $y_p$ -axis and  $B_p$ , the projection of the spin axis onto the horizontal:  $\alpha = \phi - \theta_2$ , with positive in the same direction as  $\phi$ . A nutation angle of  $\theta = -\pi/2$  indicates a horizontal  $B$ -axis.

The  $(A, B, C)$  coordinate system of the RNA is also positioned using the 3-1-3 sequence Euler angles  $\phi$ - $\theta$ - $\psi$ , as shown in Fig. 2. The  $(X_n, Y_n, Z_n)$  coordinate system has translation relative to the earth and shares the same origin with  $(A, B, C)$ . The angular transformation from  $(X_n, Y_n, Z_n)$  to  $(A, B, C)$  is the order of: 1) rotate the disk coordinate system  $(A, B, C)$  about the  $z_n$ -axis by an angle  $\phi$  in the  $X_n$ - $Y_n$  plane; 2) next rotate about the resulting  $C$ -axis by an angle  $\theta$ , and then finally 3) rotate

about the resulting  $B$ -axis by an angle  $\psi$ . In this 3-1-3 sequence, precession and spin are applied along the same moving axis, since the initial  $B$ -axis coincides with the  $z_n$ -axis. The angular velocity components of precession, nutation and spin are Euler angular velocities  $\dot{\phi}$ ,  $\dot{\theta}$  and  $\dot{\psi}$ , each with positive as a right-hand rotation about its rotation axis. Similar to the  $(x, y, z)$  system, the  $(A, B, C)$  system is not body-fixed.  $(A_1, B, C_1)$  is an exact body-fixed coordinate system on the RNA and has spinning motion relative to  $(A, B, C)$ . This definition of the  $(A, B, C)$  coordinate system greatly simplifies derivation of Euler kinematics equations of the RNA and computation of gyroscopic moments.

### 3 Connecting the two sets of Euler Angles

Motion of the tower is described by Euler rotations  $\theta_2$ ,  $\theta_1$ , and  $\eta$ , while RNA rotations are described by  $\phi$ ,  $\theta$ , and  $\psi$ . These two sets of angles describe bodies that are physically connected in space, so the number of degrees of freedom can be reduced by expressing the motion of the RNA in terms of  $\theta_1$ ,  $\theta_2$ , and  $\eta$  using vector projection. Fig. 3 shows both  $(A, B, C)$  and  $(x, y, z)$  coordinate systems, which are relocated to the origin,  $O$ , for convenience.

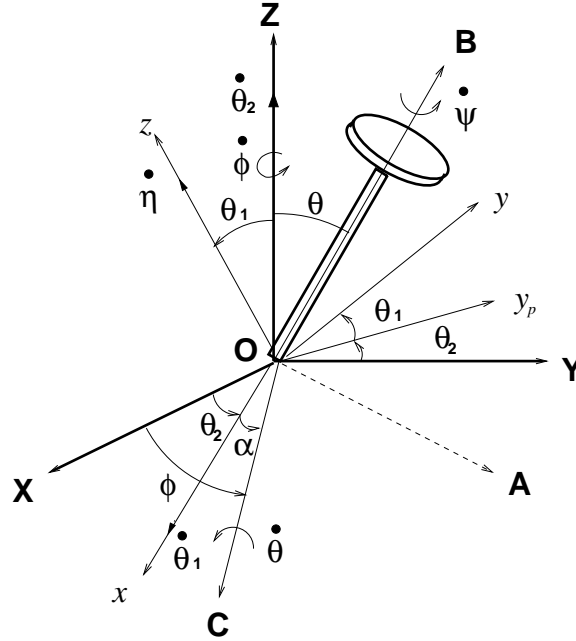


Fig. 3. Projection of Euler angular velocities

#### 3.1 Nutation:

The nutation angular velocity and acceleration are obtained by projecting  $\dot{\theta}_1$ ,  $\dot{\theta}_2$  and  $\dot{\eta}$  onto the  $C$ -axis and differentiating:

$$\dot{\theta} = \dot{\theta}_1 \cos \angle COx + \dot{\theta}_2 \cos \angle COZ + (\dot{\eta} + \omega_{yaw}) \cos \angle COz \quad (1)$$

$$= \dot{\theta}_1 \cos \alpha - (\dot{\eta} + \omega_{yaw}) \sin \theta_1 \sin \alpha \quad (2)$$

$$\begin{aligned} \ddot{\theta} = & \ddot{\theta}_1 \cos \alpha - \dot{\theta}_1 \dot{\alpha} \sin \alpha - (\dot{\eta} + \dot{\omega}_{yaw}) \sin \theta_1 \sin \alpha \\ & - (\dot{\eta} + \omega_{yaw})(\dot{\theta}_1 \cos \theta_1 \sin \alpha + \dot{\alpha} \sin \theta_1 \cos \alpha) \end{aligned} \quad (3)$$

where  $\omega_{yaw}$  is yaw rate, angular motion of the RNA relative to the tower along  $z$ -axis, and  $\dot{\omega}_{yaw}$  is its time derivative. The nutation angle,  $\theta$ , has been obtained geometrically in separate work by the authors [11], which is more accurate than numerical integration of  $\dot{\theta}$  in Eqn. (2), and decreases the required number of degrees of freedom:

$$\theta = -\frac{\pi}{2} + \lambda \quad (4)$$

$$= -\frac{\pi}{2} + \arctan(\tan \theta_1 \cos(\phi - \theta_2)) \quad (5)$$

where  $\lambda$  is the angle between the  $B$ - and  $B_p$ -axes.

### 3.2 Precession:

The derivation of the precession angular velocity,  $\dot{\phi}$ , is based on the definition of yaw rate:

$$\omega_{yaw} = \omega_{z,RNA} - \omega_{z,tower} \quad (6)$$

where  $\omega_{z,RNA}$  is the absolute angular velocity of the RNA about the  $z$ -axis and can be obtained by projection of Euler angular velocities  $\dot{\phi}$ ,  $\dot{\theta}$  and  $\dot{\psi}$  onto the  $z$ -axis;  $\omega_{z,tower}$  is the absolute angular velocity of the tower about the  $z$ -axis and can be obtained by the projection of Euler angular velocities  $\dot{\theta}_1$ ,  $\dot{\theta}_2$  and  $\dot{\eta}$  onto the  $z$ -axis:

$$\omega_{z,tower} = \dot{\theta}_1 \cos \angle xOz + \dot{\theta}_2 \cos \angle ZOz + \dot{\eta} \quad (7)$$

$$\omega_{z,RNA} = \dot{\phi} \cos \angle ZOz + \dot{\theta} \cos \angle COz + \dot{\psi} \cos \angle BOz \quad (8)$$

Considering Fig. 3,  $\cos \angle ZOz = \cos \theta_1$  and  $\cos \angle xOz = \cos \angle BOz = \cos(\pi/2)$ . The vertical plane  $zOy_p$  is perpendicular to the horizontal plane  $COy_p$ , so  $\angle COz$  can be shown to be:

$$\begin{aligned} \cos \angle COz &= \cos \angle zOy_p \cos \angle COy_p \\ &= \cos\left(\frac{\pi}{2} + \theta_1\right) \cos\left(\frac{\pi}{2} - \alpha\right) \\ &= -\sin \theta_1 \sin \alpha \end{aligned} \quad (9)$$

Substituting Eqns. (7) and (8) into Eqn. (6) yields the precession velocity:

$$\dot{\phi} = (\cos^2 \theta_1 + \sin^2 \theta_1 \cos^2 \alpha) \sec \theta_1 (\omega_{yaw} + \dot{\eta}) + \quad (10)$$

$$\dot{\theta}_2 + \dot{\theta}_1 \tan \theta_1 \sin \alpha \cos \alpha \quad (11)$$

Eqn. (11) can alternatively be derived by differentiating Eqn. (5) and equating the resulting  $\dot{\theta}$  with Eqn. (2). Setting  $\omega_{yaw} = 0$  in Eqn. (11) shows that precession velocity,  $\dot{\phi}$ , is a function of overall tower motions; further assuming relatively small  $\theta_1$ , Eqn. (11) can be reduced to  $\dot{\phi} \approx \dot{\theta}_2 + \dot{\eta} \cos \theta_1$ , which helps to clarify the relationship between  $\theta_2$  and  $\eta$ . Differentiating Eqn. (11) yields the precession acceleration:

$$\begin{aligned} \ddot{\phi} &= (\omega_{yaw} + \dot{\eta})(\dot{D} \sec \theta_1 + D \sec \theta_1 \tan \theta_1 \dot{\theta}_1) + \\ &(\omega_{yaw} + \dot{\eta})D \sec \theta_1 + \ddot{\theta}_2 + \dot{\theta}_1 \dot{\alpha} \cos 2\alpha \tan \theta_1 + \\ &\frac{1}{2}(\ddot{\theta}_1 \tan \theta_1 \sin 2\alpha + \dot{\theta}_1^2 \sec^2 \theta_1 \sin 2\alpha) \end{aligned} \quad (12)$$

in which  $D = \cos^2 \theta_1 + \sin^2 \theta_1 \cos^2 \alpha$  and  $\dot{D} = -\dot{\theta}_1 \sin^2 \alpha \sin 2\theta_1 - \dot{\alpha} \sin^2 \theta_1 \sin 2\alpha$

### 4 Equation of Motion of the Tower

Beginning at first principles, the sum of the moments resulting from externally applied forces about the center of mass of a body in a translating-rotating system,  $(x, y, z)$ , equals the change of the momentum within the coordinate system plus that associated with the movement of the coordinate system (e.g. [10]):

$$\sum \vec{M} = \dot{\vec{H}}_O = (\dot{\vec{H}}_O)_{xyz} + \vec{\Omega} \times \vec{H}_O \quad (13)$$

Vector  $\vec{\Omega}$  describes the angular velocity of  $(x, y, z)$  with respect to  $(X, Y, Z)$ . The  $x$ -,  $y$ - and  $z$ -axes are chosen as the principal axes of the body, so the products of inertia in  $\vec{H}_O$  disappear, and locating the coordinate system at the center of mass decouples the rotational and translational degrees of freedom. For the one-body problem, this decoupling enables solution

of the rotational degrees of freedom without regard for the translational. Following e.g. Hibbeler [10], Eqn. (13) expands to three scalar equations:

$$\sum M_x = I_x \dot{\omega}_x - I_y \omega_y \Omega_z + I_z \omega_z \Omega_y \quad (14)$$

$$\sum M_y = I_y \dot{\omega}_y - I_z \omega_z \Omega_x + I_x \omega_x \Omega_z \quad (15)$$

$$\sum M_z = I_z \dot{\omega}_z - I_x \omega_x \Omega_y + I_y \omega_y \Omega_x \quad (16)$$

where  $\vec{\omega}$  describes the rotation of the tower in space. The more conventional form of Eqns (14)–(16) has  $\vec{\omega} = \vec{\Omega}$ , such that the coordinate system is fixed to the body. The difference between motion of the  $(x, y, z)$  coordinate system,  $\vec{\Omega}$ , and that of the body,  $\vec{\omega}$ , is the Euler angle  $\eta$ :  $\vec{\omega} = \vec{\Omega} + \dot{\eta} \vec{k}$ . The associated Euler kinematic equations are:

$$\vec{\omega} = \omega_x \vec{i} + \omega_y \vec{j} + \omega_z \vec{k} \quad (17)$$

$$= \dot{\theta}_1 \vec{i} + (\dot{\theta}_2 \sin \theta_1) \vec{j} + (\dot{\theta}_2 \cos \theta_1 + \dot{\eta}) \vec{k} \quad (18)$$

Continuing to follow e.g. [10], component-wise expressions for  $\vec{\omega}$ ,  $\dot{\vec{\omega}}$  and  $\vec{\Omega}$  are substituted into a component-wise expansion of Eqn. (13). Principal moments of inertia of the tower,  $I_x$ ,  $I_y$  and  $I_z$ , are taken about the  $x$ -,  $y$ - and  $z$ -axes. The tower is symmetrical such that  $I_x = I_y = I$ . The resulting Euler dynamic equations are:

$$\sum M_x = I(\ddot{\theta}_1 - \dot{\theta}_2^2 \sin \theta_1 \cos \theta_1) + I_z \dot{\theta}_2 \sin \theta_1 (\dot{\theta}_2 \cos \theta_1 + \dot{\eta}) \quad (19)$$

$$\sum M_y = I(\ddot{\theta}_2 \sin \theta_1 + 2\dot{\theta}_1 \dot{\theta}_2 \cos \theta_1) - I_z \dot{\theta}_1 (\dot{\theta}_2 \cos \theta_1 + \dot{\eta}) \quad (20)$$

$$\sum M_z = I_z(\ddot{\eta} + \dot{\theta}_2 \cos \theta_1 - \dot{\theta}_1 \dot{\theta}_2 \sin \theta_1) \quad (21)$$

The moments on the left hand side of Eqns. (19)–(21) are externally applied about the center of mass of the tower.

$$\sum M_x = M_{RNAx} + M_{FTx} + M_{wavex} - M_{mooringx} - M_{hydrostatic} \quad (22)$$

$$\sum M_y = M_{RNAy} + M_{FTy} + M_{wavey} - M_{mooringy} \quad (23)$$

$$\sum M_z = M_{RNAz} + M_{FTz} + M_{wavez} - M_{mooringz} \quad (24)$$

where  $\vec{M}_{RNA}$  represents the total moment applied by the RNA on the top of the tower;  $\vec{M}_{FT}$  is the total moment resulting from the RNA forces, those forces applied to the top of the tower by the RNA:  $\vec{M}_{FT} = \vec{r} \times \vec{F}_T$ . Vector  $\vec{r}$  is from the mass center of the tower to the RNA; the RNA forces,  $\vec{F}_T = \vec{F}_b - m_R \vec{a}_R$ , where  $m_R$  is the mass of the RNA, and  $\vec{a}_R$  is the linear acceleration of the RNA caused by rotation of the tower. This acceleration,  $\vec{a}_R$ , is the derivative of the velocity at the top of the tower;  $\vec{F}_b$  is the thrust force on the blade area.  $\vec{M}_{wave}$  is the hydrodynamic forcing. The mooring restoring moment,  $\vec{M}_{mooring}$ , can be calculated as a sum of cross-products, with each mooring line represented by a cross-product between the radius vector from the center of mass of the tower to the fairlead and the force vector. Hydrostatic restoring moment,  $\vec{M}_{hydrostatic}$ , is generally zero in the  $y$ - and  $z$ -directions.

## 5 Moments caused by Rotational Motion of the RNA

Rotational motions of the RNA are treated the same way as the rotational equations of motion of the tower in Section 4: as a single rigid body using the 3-1-3 Euler sequence, with the body rotating separately from the rotating coordinate system. The rotational motion of the RNA differs from that of the coordinate system  $(A, B, C)$  only by the spinning rate along the  $B$ -axis:

$$\vec{\omega} = \omega_A \vec{i}_{ABC} + \omega_B \vec{j}_{ABC} + \omega_C \vec{k}_{ABC} \quad (25)$$

$$= (\dot{\phi} \sin \theta) \vec{i}_{ABC} + (\dot{\phi} \cos \theta + \dot{\psi}) \vec{j}_{ABC} + \dot{\theta} \vec{k}_{ABC} \quad (26)$$

where  $\vec{i}_{ABC}$ ,  $\vec{j}_{ABC}$  and  $\vec{k}_{ABC}$  are unit vectors along the  $A$ -,  $B$ - and  $C$ -axes.

Following a derivation similar to Section 4, the resulting Euler dynamic equations can be applied to compute the RNA moments applied by the tower on the RNA:

$$M_A = I_A(\ddot{\phi} \sin \theta + 2\dot{\theta}\dot{\phi} \cos \theta) - I_B\dot{\theta}(\dot{\psi} + \dot{\phi} \cos \theta) \quad (27)$$

$$M_B = I_B(\ddot{\phi} \cos \theta - \dot{\theta}\dot{\phi} \sin \theta) - M_{windB} \quad (28)$$

$$M_C = I_C(\ddot{\theta} - \dot{\phi}^2 \sin \theta \cos \theta) + I_B\dot{\phi} \sin \theta(\dot{\psi} + \dot{\phi} \cos \theta) \quad (29)$$

The moments of inertia are those of a rigid body representing the RNA; the parts of the RNA not rotating at  $\dot{\psi}$  are assumed to be a point-mass on the  $B$ -axis. Moments  $I_A$  and  $I_C$  are about the  $A$ - and  $C$ -axes, and  $I_B$  can realistically be taken as the moment of inertia of the blades about  $B$ . Contributions to  $M_A$  and  $M_C$  due to asymmetrical external forcing are neglected, such as asymmetric wind loading. The non-zero  $M_{windB}$  is the rotor torque used to generate electricity. The spin velocity is assumed constant,  $\dot{\psi} = 0$ , in accordance with typical wind turbine operations.

Any terms in Eqns. (27)-(29) including spin,  $\dot{\psi}$ , which disappear when the rotor is parked, are the gyroscopic moments:

$$M_{gyroA} = -I_B\dot{\theta}\dot{\psi} \quad (30)$$

$$M_{gyroB} = 0 \quad (31)$$

$$M_{gyroC} = I_B\dot{\phi} \sin \theta \dot{\psi} \quad (32)$$

The gyro moments of bottom-fixed wind turbine can be estimated as those corresponding to a static, upright tower. Considering only the gyroscopic moments and substituting  $\theta = -\frac{\pi}{2}$  and  $\dot{\theta} = 0$  into Eqns. (27)-(29) yields precisely the results given by e.g. Henderson [1] when  $\theta_1$  motion is neglected. On large bottom-founded turbines, gyroscopic moments are limited by active yaw control such that the precession angular velocity remains small. On compliant floating turbines, however, significant gyroscopic moments can be developed about the  $A$ - and  $C$ -axes. The  $A$ -axis lies nearly along the axis of the tower, with  $M_{gyroA}$  moments resulting from nutation of the RNA, as noted by Jonkman [6].

The RNA moments must be transformed from the  $(A, B, C)$  coordinate system into the  $(x, y, z)$  system for application in the equations of motion of the tower:

$$\begin{bmatrix} M_{RNAx} \\ M_{RNAy} \\ M_{RNAz} \end{bmatrix} = T \begin{bmatrix} -M_C \\ -M_A \\ -M_B \end{bmatrix} \quad (33)$$

The transformation matrix  $T$  is obtained by first rotating  $(x, y, z)$  back to the  $(X, Y, Z)$  system and then rotating from  $(X, Y, Z)$  to the final  $(C, A, B)$  rotational system (Fig. 3). The  $(X, Y, Z)$  and  $(x, y, z)$  systems translate together with the tower, so translation does not influence the transformation matrix. The transformation matrix from the  $(C, A, B)$  to  $(x, y, z)$  results from the product of a sequence of element rotation matrixes:

$$T = T_{x_1}(-\theta_1)T_{x_3}(-\theta_2)T_{x_3}(\phi)T_{x_1}(\theta) \quad (34)$$

where  $T_{x_1}(-\theta_1)T_{x_3}(-\theta_2)$  indicates rotation from  $(x, y, z)$  back to initial  $(X, Y, Z)$ , in which both the ordering of rotation and the directions of the rotational angles must be reversed. Element rotation matrixes  $T_{x_1}$  and  $T_{x_3}$  are defined in Section 7.

## 6 Transformation of Moments resulting from RNA Forces

The environmental and inertial forcing in Eqns. (22)-(24) can be computed considering both the wind and waves acting on the structure, and the relative motion of the tower through the air and water. The linear velocity of the RNA through the air is computed from the angular velocities:

$$\vec{v}_{\theta_1} = \dot{\theta}_1 \times \vec{r}_s = \dot{\theta}_1 l \quad (35)$$

$$\vec{v}_{\theta_2} = \dot{\theta}_2 \times \vec{r}_s = \dot{\theta}_2 l \sin \theta_1 \quad (36)$$

where  $\vec{v}_{\theta_1}$  and  $\vec{v}_{\theta_2}$  are linear-velocity components at a location along the  $z$ -axis (here, the RNA); angular velocity  $\dot{\theta}_1$  is along the negative direction of the  $y$ -axis and  $\dot{\theta}_2$  is along the positive direction of the  $x$ -axis. In Fig. 4, vector  $\vec{r}_s$  is the radius from

the center of mass of the system,  $O_s$ , to that location, and  $l$  is the magnitude of  $\vec{r}_s$ . Direction vectors  $(i_l, j_l, k_l)$  and  $(i, j, k)$  are along  $(X, Y, Z)$  and  $(x, y, z)$  respectively. Linear acceleration of the RNA is needed to calculate the RNA forces,  $F_T$ . This acceleration,  $\vec{a}_R$ , is computed by taking the derivative of the vector sum of  $\vec{v}_{\theta_1}$  and  $\vec{v}_{\theta_2}$  and then transforming into the  $(x, y, z)$  coordinate system.

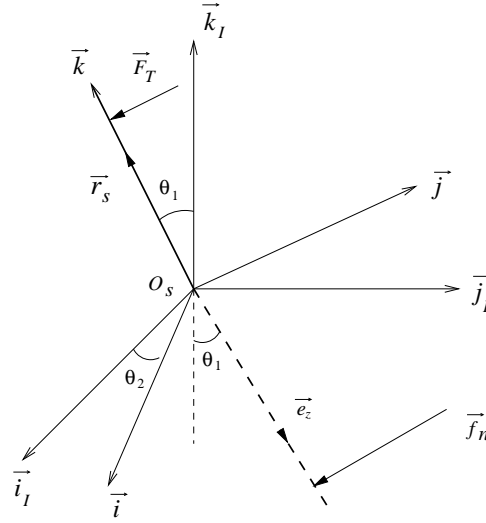


Fig. 4. Coordinate system for derivation of inertial and environmental forcing

An expression for the velocity of the wind relative to the RNA,  $V_{rb}$ , along the negative  $B$ -axis, can be developed from Eqns. (35) and (36) and direction cosines, which can be derived geometrically or through use of transformation matrices:

$$\vec{V}_{rb} = \vec{v}_w + \vec{v}_{\theta_1}(-\cos \angle BOy) + \vec{v}_{\theta_2} \cos \angle BOx \quad (37)$$

$$V_{rb} = -v_w + \dot{\theta}_1 l (\cos \theta_1 \sin \theta \cos \alpha - \cos \theta \sin \theta_1) + \dot{\theta}_2 l \sin \theta_1 \sin \theta \sin \alpha \quad (38)$$

where  $v_w = |\vec{v}_w|$  and is along the negative  $B$ -axis. The resulting relative velocity can be used to compute the wind forces acting on the RNA in the  $(X, Y, Z)$  coordinate system, after which they must be transformed into the  $(x, y, z)$  system for application in the equations of motion. Moments resulting from RNA forces include both wind and inertial loads.

$$\vec{M}_{FT} = \vec{r} \times \vec{F}_T = \vec{r} \times (\vec{F}_b - m_R \vec{a}_R) = \vec{M}_{wind} - \vec{r} \times m_R \vec{a}_R \quad (39)$$

where  $\vec{r}$  originates at the center of mass of the tower. The wind moments result from decomposing the thrust force,  $\vec{F}_b$ , onto the  $(x, y, z)$  system, and calculating moments as a cross product expressed as a cofactor expansion:

$$\vec{M}_{wind} = \vec{r} \times \vec{F}_b = \begin{bmatrix} \vec{i} & \vec{j} & \vec{k} \\ 0 & 0 & l \\ -F_b \cos \angle BOx & -F_b \cos \angle BOy & -F_b \cos \angle BOz \end{bmatrix} \quad (40)$$

## 7 Transformations for Wave Forcing

Similar to the calculation of wind forcing, wave forces are computed in the  $(X, Y, Z)$  coordinate system, decomposed into the  $(x, y, z)$  system, and used to compute the moments. Waves are assumed to progress down the negative  $Y$ -axis. The wave kinematic velocity relative to the moving tower is  $\vec{V}_{rt}$ . Determination of  $\vec{V}_{rt}$  requires expression of velocity vectors for both the tower and the wave kinematics normal to the axis of the tower in the  $(X, Y, Z)$  coordinate system. In general, 3-D rotation matrices of a regular right-handed  $(x_1, x_2, x_3)$  coordinate system can be expressed in a general form e.g. [12]. Here, the location of the centerline of the tower is fully defined by  $(\theta_1, \theta_2)$ , with the final rotation about the  $z$ -axis being irrelevant, so the transformation matrix from  $(x, y, z)$  to  $(X, Y, Z)$  can be computed from the general form as in [11].

$$T_{x_3}(\theta_2)T_{x_1}(\theta_1) = \begin{bmatrix} \cos \angle XOx & \cos \angle XOy & \cos \angle XOz \\ \cos \angle YOx & \cos \angle YOy & \cos \angle YOz \\ \cos \angle ZOx & \cos \angle ZOy & \cos \angle ZOz \end{bmatrix}$$

$$T_Z(\theta_2)T_x(\theta_1) = \begin{bmatrix} \cos\theta_2 - \cos\theta_1 \sin\theta_2 & \sin\theta_1 \sin\theta_2 \\ \sin\theta_2 & \cos\theta_1 \cos\theta_2 & -\cos\theta_2 \sin\theta_1 \\ 0 & \sin\theta_1 & \cos\theta_1 \end{bmatrix} \quad (41)$$

The instantaneous unit vector along the negative  $z$ -axis can be deduced directly from Fig. 4:

$$\vec{e}_z = -\cos\angle XOz\vec{i}_I - \cos\angle YOz\vec{j}_I - \cos\angle ZOz\vec{k}_I \quad (42)$$

The direction cosines appear as matrix elements in Equation 41. The unit vector  $\vec{e}_z$  can then be used to find the relative normal velocity:

$$\vec{V}_n = \vec{e}_z \times (\vec{V}_r \times \vec{e}_z) \quad (43)$$

where  $\vec{V}_r$  is the relative velocity of the wave to the submerged tower:  $\vec{V}_r = \vec{V} - \vec{V}_t$ , in which  $\vec{V} = (0, u_Y, u_Z)$  is the wave kinematic velocity in the  $YOZ$  plane.

The transformation matrix, Eqn. (41), is again used to compute the structural velocity,  $\vec{V}_t$ . Linear velocities  $\vec{v}_{\theta_1}$  and  $\vec{v}_{\theta_2}$ , are found as in Eqns. (35) and (36), with  $\vec{r}_s$  originating at the center of mass of the system and now along the negative direction of the  $z$ -axis of the submerged tower, such that linear velocity  $\vec{v}_{\theta_1}$  is along the positive direction of the  $y$ -axis and  $\vec{v}_{\theta_2}$  is along the negative direction of the  $x$ -axis. Decomposing into the  $(X, Y, Z)$  system:

$$\begin{aligned} \vec{V}_t &= \vec{v}_{\theta_1, XYZ} + \vec{v}_{\theta_2, XYZ} \\ &= (\vec{v}_{\theta_1} \cos\angle XOy - \vec{v}_{\theta_2} \cos\angle XOx)\vec{i}_I \\ &\quad + (\vec{v}_{\theta_1} \cos\angle YOy - \vec{v}_{\theta_2} \cos\angle YOx)\vec{j}_I \\ &\quad + (\vec{v}_{\theta_1} \cos\angle ZOy - \vec{v}_{\theta_2} \cos\angle ZOx)\vec{k}_I \end{aligned} \quad (44)$$

$$(45)$$

It may also be useful to know the absolute kinematic wave-particle acceleration in absence of tower motion,  $\dot{\vec{V}}_n$ . Similar to Eqn. (43), the normal component of wave acceleration,  $\dot{\vec{V}}_n$ , can be expressed as:

$$\dot{\vec{V}}_n = \vec{e}_z \times (\dot{\vec{V}} \times \vec{e}_z) \quad (46)$$

where  $\dot{\vec{V}} = (0, \dot{u}_Y, \dot{u}_Z)$  is the wave acceleration vector in the  $YOZ$  plane.

Wave moments in the  $(x, y, z)$  coordinate system necessary for application in the Euler equations of motion can be computed using the relative velocities and accelerations resulting from Eqns. (43) and (46) at finite slices of the cylinder, then transforming the resulting forces into the  $(x, y, z)$  system (Eqn. (41)) and numerically integrating over the submerged length of the tower:

$$\vec{f}_{n,xyz} = [T_Z(\theta_2)T_x(\theta_1)]^{-1} \vec{f}_n \quad (47)$$

$$\vec{M}_{wave} = \int_r (\vec{r} \times \vec{f}_{n,xyz}) dr \quad (48)$$

$$\vec{M}_{wave} = M_{wavex}\vec{i} + M_{wavey}\vec{j} + M_{wavez}\vec{k} \quad (49)$$

where  $M_{wavex}$ ,  $M_{wavey}$  and  $M_{wavez}$  are three components of the moments of wave forces in the  $(x, y, z)$  coordinate system. In practice, the integral in Eqn. (48) is computed as a finite sum. Use of relative velocities in computation of wave forcing introduces damping in the  $\theta_1$ - and  $\theta_2$ -directions.

## 8 Example

The motions and RNA loads of a floating wind turbine are simulated using this implementation which applies the existing ODE45 solver in MATLAB. The example is based on the OC3 Hywind model [13], with the hull modified to allow large-amplitude motion. The RNA is the same as that of OC3 Hywind: the moments of inertia of the RNA about

the  $(A, B, C)$  coordinate system are  $I_A = 2.35 \times 10^7 \text{ kg}\cdot\text{m}^2$ ,  $I_B = 4.37 \times 10^7 \text{ kg}\cdot\text{m}^2$ ,  $I_C = 2.54 \times 10^7 \text{ kg}\cdot\text{m}^2$ ; the rotor speed is 12.1 rpm. Additional yaw stiffness of  $9.834 \times 10^7 \text{ N}\cdot\text{m}/\text{rad}$  is added to be consistent with Hywind model.

Modifications to the standard Hywind model were made to enable large amplitude motion and to simplify the simulation. To increase rotational motions, the submerged length of the spar hull is reduced from 120 m to 72 m. The tower between the hull and RNA is treated as a rigid body and its moments of inertia are combined with those of the hull:  $3.57 \times 10^9 \text{ kg}\cdot\text{m}^2$  and  $9.28 \times 10^7 \text{ kg}\cdot\text{m}^2$  in the tilt (roll or pitch) and yaw, respectively. The four taught-leg mooring lines are each assumed to be a straight axial spring with stiffness  $EA = 3.84 \times 10^8 \text{ N}$  and length 409 m in a 320 m water depth location.

The first example case presented is free-vibration in absence of environmental loading; the second is forced-vibration with environmental loading computed using irregular winds and waves. Irregular wind velocities are simulated by IECwind [14] and Turbsim [15]. The mean wind velocity at hub height is 18.2 m/s. The thrust force due to wind on the blade area is computed as a function of thrust coefficient,  $C_T$ , times relative velocity squared. Here, the value of  $C_T$  depends solely on relative wind velocity and is taken directly from Nielsen [16]. The thrust coefficient generally decreases with increasing relative wind speed and is assumed to change instantaneously. The steady moment along the  $B$ -axis that generates electricity,  $M_{windB}$ , is estimated by dividing the rated efficiency of turbine by  $\psi$  (Eqn. (28)). Wave forces are computed using the Morison equation and a first-order time-domain representation of irregular waves is simulated directly from a JONSWAP spectrum with a significant wave height of 5.0 m and peak period of 11.2 s using a uniform phase distribution.

The thrust force for wind perpendicular to the swept area of the blades is approximately (e.g., [16]):

$$F_b = \frac{1}{2} C_T \rho_a A_b V_{rb}^2 \quad (50)$$

where  $\rho_a$  is the density of air;  $A_b$  is the swept area of the blades;  $C_T$  is the thrust coefficient. The force is in the direction of  $V_{rb}$ , the velocity of the wind relative to the RNA along the negative  $B$ -axis.

Wave loads are estimated using the well-known Morison equation in the  $(X, Y, Z)$  system (e.g., [17]):

$$\vec{f}_n = C_m \rho \frac{\pi}{4} D^2 \dot{\vec{V}}_n - C_a \rho \frac{\pi}{4} D^2 \dot{\vec{V}}_t + \frac{1}{2} \rho C_d D \vec{V}_{rt} |\vec{V}_{rt}| \quad (51)$$

where  $\rho$  is the density of sea water;  $D$  is the diameter of the tower;  $C_m = 2.0$  is the inertia coefficient;  $C_a = 1.0$  is the added mass coefficient, and  $C_d = 0.6$  is the drag coefficient. All velocities, accelerations and forces are normal to the central axis of the tower:  $\vec{f}_n$  is the wave force per unit length of the tower (Fig. 4). The kinematic acceleration normal to the axis of the tower is  $\dot{\vec{V}}_n$ . The second acceleration term, which includes the tower acceleration  $\dot{\vec{V}}_t$ , is technically a force resulting from a hydrodynamic pressure, but this term effectively has been moved to the inertial side of the equation as the basis for calculation of added mass. Added mass is included in the calculation of the center of mass and moment of inertia of the body, and so should not be included here. The result is that the relative velocity,  $\vec{V}_{rt}$ , is applied in the Morison drag term, but the absolute acceleration,  $\dot{\vec{V}}_n$ , is applied in the acceleration term. Damping in the  $z$ -direction can be added directly to the R.H.S. of Eqn. (24).

### 8.1 Verification for small angles

This case directly compares results from the large-angle theory presented here with the small-angle theory applied in FAST. The observed undamped free-vibration results from initial conditions of a  $\theta_1$  offset of 0.1 rad and zero  $\theta_2$ . The resulting motion corresponds to an inverted pendulum moving in a single nearly-vertical plane; the plane is not exactly vertical because Hywind has the center of mass of the RNA slightly offset from the tower centerline. Representation of precisely the same physical system in both models is enabled by replacing the default restoring moment calculations in FAST with a user subroutine that was custom-developed to yield identical hydrostatic and mooring stiffness, and by turning off the translational motion calculations in FAST. Fig. 5 shows resulting time-histories for  $\theta_1$ ,  $\theta_2$  and  $\eta$ . The 3-1-3 Euler sequence does not admit negative values of  $\theta_1$ , so the tower passing through vertical is consistent with  $\pi$  rad jumps in  $\theta_2$ ; similar results are found by e.g. [18]. Direct comparison of Euler-angle results is impossible because FAST computes roll, pitch and yaw about an earth fixed coordinate system. Simulation results can be directly compared by projecting angular velocities onto the earth-fixed coordinate system, as shown in Fig. 6 and Fig. 7. Results show excellent agreement for this small-angle case.

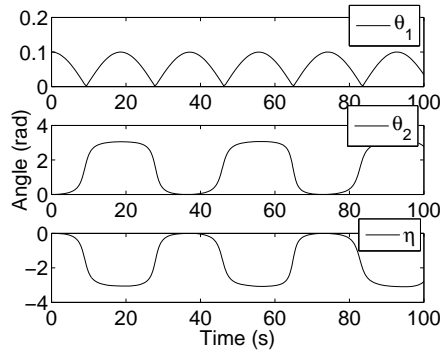


Fig. 5. Case 1: Free vibration described by three Euler angles

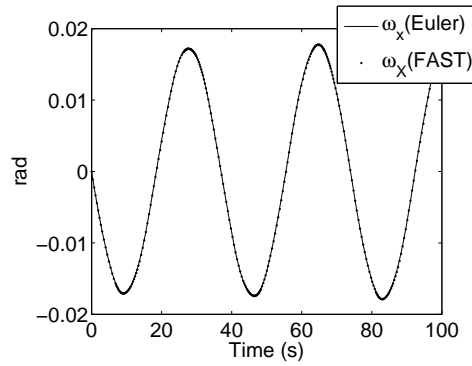


Fig. 6. Case 1: Comparison of  $\omega_x$

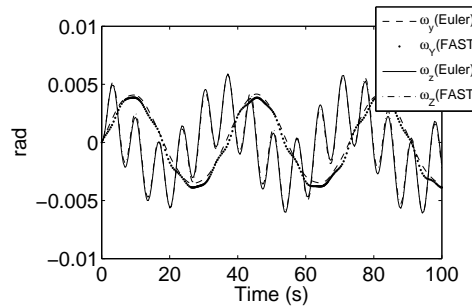


Fig. 7. Case 1: Comparisons of  $\omega_y$  and  $\omega_z$

## 8.2 Yaw of the RNA

This case is used to investigate the behavior of the dynamic system subject to irregular winds, waves and a large wind shift. The wind time-history is generated by superimposing a time-history of a sudden 45 degree shift from IECwind [14] at a time 100 seconds into an irregular operating condition from Turbsim [15]. A typical yaw control algorithm is assumed, which includes a 10-second lag before yaw activation and a 10-second acceleration or deceleration period. Fig. 8 shows precession of the RNA. In case of gust, precession angle is dominated by yaw of the RNA, which is active from 110 seconds to about 260 seconds, when the precession angle of the RNA changes from 0 rad to about 0.8 rad. Fig. 9 shows the gyro moments in the A- and C-directions. For a conventional bottom-fixed turbine,  $M_{gyroA} = 0$  because the spin axis remains horizontal and  $M_{gyroC}$  is dominated by the mechanical precession velocity (Eqns. 27–29 with  $\theta = -\pi/2$ ). For this compliant floating structure, however, the precession velocity is dominated by tower motions rather than yaw of the RNA relative to the tower. Tower-motion induced gyro moments can be substantial. Continuous operation of the yaw control mechanism to offset tower motions could minimize these moments, but such control would require a wholly new yaw control strategy.

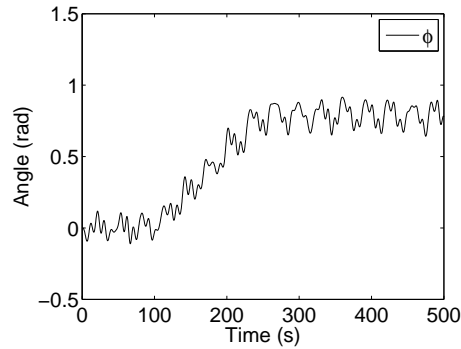


Fig. 8. Precession angle of the RNA

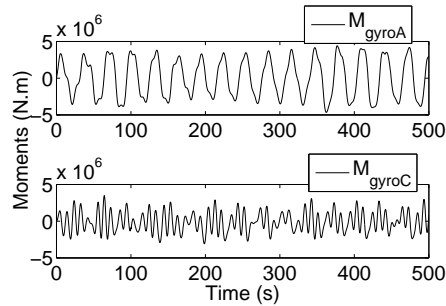


Fig. 9. Gyro moments acting on the RNA

## 9 Conclusions

A new method has been developed to apply Euler dynamic equations in a 3-1-3 sequence to the motion of a floating wind turbine. The tower and RNA are considered as two rotational bodies in the space, for which two sets of Euler angles are defined and used to develop two systems of Euler dynamic equations of motion. The number of degrees of freedom is reduced by using the geometric constraints of the physical joint between the tower and RNA to express one set of Euler angles as a function of the other. Full dynamic coupling is preserved through the loads on the interface between the two bodies (the RNA loads), which include gyroscopic moments. The new theory is implemented as part of a time-domain numerical simulation methodology, which retains the full nonlinear coupling between external forcing and large-angle rotations of the tower. Motions and external forcing are transformed at each time step between the non-rotating ( $X, Y, Z$ ) and rotating ( $x, y, z$ ) using matrices developed in terms of Euler angles for the rigid body. One example demonstrates that the new methodology yields substantially identical results to the well-known FAST software for a small-angle free-vibration case. Another example shows that there are two major components of gyroscopic loading on a compliant floating structure: one due to precession velocity of the spin axis and another due to nutation velocity, both of which can be substantial. Overall, the new theory is found to be effective for computation of the very complex dynamic behavior of these structures.

## 10 Acknowledgements

This work was supported by the National Science Foundation, Division of Civil and Mechanical Systems under Agreement Number CMS-0448730. Any opinions, findings, and conclusions or recommendations expressed in this material are those of the authors and do not necessarily reflect the view of the National Science Foundation.

## References

- [1] A. R. Henderson and J. H. Vugts, "Prospects for floating offshore wind energy," in *Proceedings of the European Wind Energy Conference*, 2001.
- [2] S. Chandrasekaran and A. K. Jainb, "Dynamic behaviour of square and triangular offshore tension leg platforms under regular wave loads," *Journal of Applied Mechanics*, vol. 66, no. 4, pp. 986–996, 1999.
- [3] E. Bush, *A Comparison of Alternate Foundation Models for Offshore Wind Turbines and resulting Long-term Loads*. PhD thesis, University of Texas at Austin, 2009.
- [4] J. M. Jonkman and M. L. J. Buhl, "Fast user's guide," Tech. Rep. NREL/EL-500-38230, National Renewable Energy Laboratory, 2005.

- [5] WAMIT 4.0, *WAMIT: A Radiation-Diffraction Panel Program for Wave-Body Interactions—User’s Manual*. Dept. of Ocean Engineering, M.I.T., 1995.
- [6] J. M. Jonkman, “Dynamic modeling and loads analysis of an offshore floating wind turbine,” Tech. Rep. NREL/TP-500-41958, NREL National Energy Renewal Laboratory, 2007.
- [7] E. Stoneking, “Newton-euler dynamic equations of motion for a multi-body spacecraft,” pp. 1368–1380, AIAA Guidance, Navigation, and Control Conference, 2007.
- [8] S. Saha, “Dynamics of serial multibody systems using the decoupled natural orthogonal complement matrices,” *Journal of Applied Mechanics*, vol. 66, no. 4, pp. 986–996, 1999.
- [9] H. Matsukuma and T. Utsunomiya, “Motion analysis of a floating offshore wind turbine considering rotor-rotation,” *The IES Journal Part A: Civil and Structural Engineering*, vol. 1, no. 4, pp. 268–279, 2008.
- [10] R. C. Hibbeler, *Engineering Mechanics - Statics and Dynamics*. Pearson Prentice Hall, 2004.
- [11] B. Sweetman and L. Wang, “Large-angle rigid body dynamics of a floating offshore wind turbine using euler’s equations of motion,” NSF CMMI Research and Innovation Conference: Engineering for Sustainability and Prosperity, 2011.
- [12] D. Eberly, “Euler angle formulas,” Tech. Rep. <http://www.geometrictools.com/>, Geometric Tools, LLC, 2008.
- [13] J. Jonkman, “Definition of the floating system for phase IV of OC3,” Tech. Rep. NREL/TP-500-47535, NREL National Energy Renewal Laboratory, 2010.
- [14] D. J. Laino, “Nwtc design codes (iecwind),” Tech. Rep. <http://wind.nrel.gov/designcodes/>, National Renewable Energy Lab, 2005.
- [15] B. J. Neil Kelley, “NWTC design codes (Turbsim),” Tech. Rep. <http://wind.nrel.gov/designcodes/>, National Renewable Energy Lab, 2008.
- [16] F. G. Nielsen, T. D. Hanson, and B. Skaare, “Integrated dynamic analysis of floating offshore wind turbines,” in *Proceedings of the international Conference on Offshore Mechanics and Arctic Engineering*, 2006.
- [17] T. Sarpkaya and M. Issacson, *Mechanics of Wave Forces on Offshore Structures*. Van Nostrand Reinhold Company, 1981.
- [18] A. Guran, “Studies in spatial motion of a gyro on an elastic-foundation,” *Journal of Mechanics of Structures and Machines*, vol. 21, no. 1, pp. 185–199, 1993.